

## THE ADVANCED CAMERA FOR SURVEYS NEARBY GALAXY SURVEY TREASURY. VI. THE ANCIENT STAR-FORMING DISK OF NGC 404

BENJAMIN F. WILLIAMS<sup>1</sup>, JULIANNE J. DALCANTON<sup>1</sup>, KAROLINE M. GILBERT<sup>1</sup>, ADRIENNE STILP<sup>1</sup>, ANDREW DOLPHIN<sup>2</sup>, ANIL C. SETH<sup>3,5</sup>, DANIEL WEISZ<sup>4</sup>, AND EVAN SKILLMAN<sup>4</sup>

<sup>1</sup> Department of Astronomy, Box 351580, University of Washington, Seattle, WA 98195, USA; ben@astro.washington.edu, jd@astro.washington.edu, stephanie@astro.washington.edu, roskar@astro.washington.edu

<sup>2</sup> Raytheon, 1151 E. Hermans Road, Tucson, AZ 85706, USA; dolphin@raytheon.com

<sup>3</sup> Harvard-Smithsonian Center for Astrophysics, 60 Garden Street, Cambridge, MA 02138, USA; aseth@cfa.harvard.edu

<sup>4</sup> Department of Astronomy, University of Minnesota, 116 Church Street SE, Minneapolis, MN 55455, USA; dweisz@astro.umn.edu, skillman@astro.umn.edu

Received 2009 December 28; accepted 2010 April 14; published 2010 May 13

### ABSTRACT

We present *HST*/WFPC2 observations across the disk of the nearby isolated dwarf S0 galaxy NGC 404, which hosts an extended gas disk. The locations of our fields contain a roughly equal mixture of bulge and disk stars. All of our resolved stellar photometry reaches  $m_{F814W} = 26$  ( $M_{F814W} = -1.4$ ), which covers 2.5 mag of the red giant branch and main-sequence stars with ages  $< 300$  Myr. Our deepest field reaches  $m_{F814W} = 27.2$  ( $M_{F814W} = -0.2$ ), sufficient to resolve the red clump and main-sequence stars with ages  $< 500$  Myr. Although we detect trace amounts of star formation at times more recent than 10 Gyr ago for all fields, the proportion of red giant stars to asymptotic giants and main-sequence stars suggests that the disk is dominated by an ancient ( $> 10$  Gyr) population. Detailed modeling of the color–magnitude diagram suggests that  $\sim 70\%$  of the stellar mass in the NGC 404 disk formed by  $z \sim 2$  (10 Gyr ago) and at least  $\sim 90\%$  formed prior to  $z \sim 1$  (8 Gyr ago). These results indicate that the stellar populations of the NGC 404 disk are on average significantly older than those of other nearby disk galaxies, suggesting that early- and late-type disks may have different long-term evolutionary histories, not simply differences in their recent star formation rates. Comparisons of the spatial distribution of the young stellar mass and FUV emission in *Galaxy Evolution Explorer* images show that the brightest FUV regions contain the youngest stars, but that some young stars ( $< 160$  Myr) lie outside of these regions. FUV luminosity appears to be strongly affected by both age and stellar mass within individual regions. Finally, we use our measurements to infer the relationship between the star formation rate and the gas density of the disk at previous epochs. We find that most of the history of the NGC 404 disk is consistent with star formation that has decreased with the gas density according to the Schmidt law. However,  $\sim 0.5$ –1 Gyr ago, the star formation rate was unusually low for the inferred gas density, consistent with the possibility that there was a gas accretion event that reignited star formation  $\sim 0.5$  Gyr ago. Such an event could explain why this S0 galaxy hosts an extended gas disk.

**Key words:** galaxies: evolution – galaxies: individual (NGC 404) – galaxies: stellar content

*Online-only material:* color figures

### 1. INTRODUCTION

While both redshift surveys and stellar population studies agree that late-type disks form the majority of their stars by  $z \sim 1$  (e.g., Ravindranath et al. 2004; Barden et al. 2005; Melbourne et al. 2007; Williams et al. 2009a), the ages of early-type disks are not as well constrained. The theoretical and high-redshift observational data suggest that the old populations of early-type disks may be systematically older than those of later-type disks. On the other hand, the morphological differences between early- and late-type disks may be of recent origin, due only to differences in star formation over the past few hundred megayears. Such a scenario has been suggested for the S0 galaxy NGC 5102 (Davidge 2008), as well as for the differences between dE’s and dIrr’s.

Unfortunately, little is known about the evolutionary history of S0 galaxies, especially in the field. Although typical S0 galaxies appear to differ significantly from E galaxies, it is not yet clear where S0 galaxies fit into the Hubble tuning fork (van den Bergh 2009) or what amount of star formation they typically contain (Temi et al. 2009). While non-interacting S0 galaxies

tend to have disks similar in thickness to those of late-type galaxies (Pohlen et al. 2004; Li et al. 2009), other properties of S0 disks differ significantly from those of late-type galaxies. For example, their color gradients are less pronounced than those of late-type disks (MacArthur et al. 2004), and S0 galaxies are typically fainter than later-type disks (van den Bergh 2009). S0 galaxies are predominantly found in galaxy clusters and are mostly stripped of H I (Poggianti et al. 2009; van den Bergh 2009), whereas field S0 galaxies like NGC 404 are less common and could be a type of post-starburst dwarf (Davidge 2008).

As the nearest face-on example of an S0 galaxy (3.05 Mpc,  $m - M_0 = 27.42 \pm 0.02$ ;  $M_K = -18.9$ ;  $A_V = 0.08$ ;  $i = 11^\circ$ ;  $V_c = 190 \text{ km s}^{-1}$ ; Dalcanton et al. 2009; Schlegel et al. 1998; del Río et al. 2004), NGC 404 has been previously studied in some detail. Although its optical morphology suggests that NGC 404 is a classic “red and dead” early-type galaxy, the center appears to have a significant young component. With long-slit spectroscopy of the galaxy core, Bouchard et al. (2010) found evidence for intermediate-aged, and old stellar populations, along with a much younger component that fades very quickly with radius. The nucleus also has a dominant 1 Gyr old population ( $\sim 50\%$  of the mass; Seth et al. 2010). UV spectroscopy also indicates some very young ( $\leq 10$  Myr)

<sup>5</sup> CfA Fellow.

stars in the galaxy center (Maoz et al. 1998). Farther out, NGC 404 has a very large ( $>20$  kpc) stellar disk that is known to be dominated by red giants (Tikhonov et al. 2003). This disk also contains a large amount of H I gas in a well-defined inner disk ( $<5$  kpc) and a warped outer disk (del Río et al. 2004), although the density of gas is low ( $< 2 \times 10^{20} M_{\odot} \text{pc}^{-2}$  throughout) and only a faint ring of star formation is detected in the far-ultraviolet (FUV; Wiklind & Henkel 1990; Thilker et al. 2010).

The origin of the gas disk of NGC 404 is somewhat mysterious. del Río et al. (2004) suggest that the disk is likely due to a recent (0.5–1 Gyr ago) merger event with a dIrr galaxy, motivated by their detection of a possible warp in the disk. However, NGC 404 is very isolated for a galaxy of its mass ( $\Theta = -1.0$ ; see Karachentsev et al. 2004, for details). With no other galaxies of any kind detected within 1 Mpc of NGC 404, such a merger is not obviously consistent with the galaxy’s environment. The gas disk could therefore simply be due to late time gas infall from filaments rather than accretion of bound objects. Furthermore, a gas disk of such low density could have a very long lifetime given the low star formation rate, suggesting that it could have been accreted far earlier. By comparing the stellar populations and gas densities, we can constrain the origin of this unusual disk.

We examine the stellar populations of NGC 404 in detail using deep observations from *Hubble Space Telescope* (HST). We determine the star formation history (SFH) of several portions of the galaxy by fitting the distribution of stars in color–magnitude diagrams (CMDs) with model distributions determined from stellar evolution isochrones (as described in Dolphin 2002). Section 2 describes our data set and analysis procedures. Section 3 discusses the results of our measurements and interprets them in the context of the gas properties and our understanding of S0 galaxies; Section 4 summarizes our conclusions. We assume a distance of 3.05 Mpc (Dalcanton et al. 2009) for conversions of angular measurements to physical distances and adopt an inclination angle  $i = 11^{\circ}$  (del Río et al. 2004) for surface density measurements. We adopt a five-year *Wilkinson Microwave Anisotropy Probe* (Dunkley et al. 2009) cosmology for all conversions between time and redshift.

## 2. DATA ACQUISITION, REDUCTION, AND ANALYSIS

### 2.1. Acquisition

From 2007 August 8 to 2007 September 20, we observed a field in the NGC 404 disk located at R.A. (2000) = 17.32325 (01:09:17.6), decl. (2000) = 35.74856 (+35:44:55) with a rotation angle  $\text{PA}_{V3} = 50.0^{\circ}$ . From 2009 February 16 to 2009 February 20, we performed shallower observations for two fields located at R.A. (2000) = 17.36697 (01:09:28.1), decl. (2000) = 35.76117 (+35:45:40) with a rotation angle  $\text{PA}_{V3} = 230.0$  and R.A. (2000) = 17.333368 (01:09:20.0), decl. (2000) = 35.70205 (+35:42:07) with a rotation angle  $\text{PA}_{V3} = 230.0$ . Figure 1 shows outlines of the fields’ locations. Our field locations were chosen to maximize the number of disk stars and avoid crowding.

In the deep field, we obtained 15 full-orbit exposures with the WFPC2 (Ford et al. 1998) through the *F606W* (wide *V*) filter, and 29 full-orbit exposures through the *F814W* (*I* equivalent) filter. These data totaled 39,000 s and 75,400 s of exposure time in *F606W* and *F814W*, respectively. In the other two fields, we obtained two orbits through *F606W*, totaling 4800 s, and four orbits through *F814W*, totaling 9600 s. All images

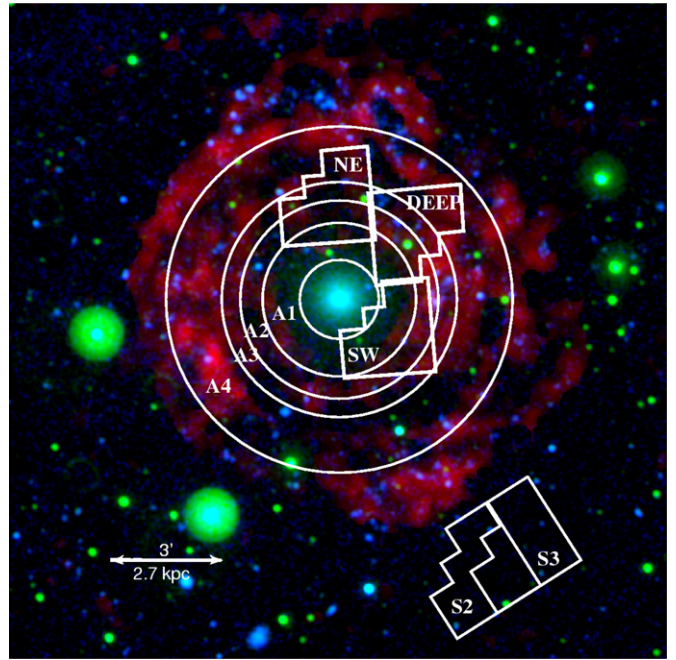


**Figure 1.** Locations of our NGC 404 fields (Section 2.1) are shown on a three-color image using *GALEX* far-UV (blue), *GALEX* near-UV (green), and H I (red) images. North is up. East is left. Fields are labeled with the names used in the text. The radial annuli used for the analysis (Section 2.5) are also shown and labeled.

were calibrated in the *HST* pipeline with CALWP2 using OPUS version 2006\_6a for the 2007 data and 2008\_5c for the 2009 data.

To expand our radial coverage, we also reduced two fields in the outer disk, previously studied and named S2 and S3 (see Tikhonov et al. 2003, for more details). These fields lie  $\sim 8'$  (7 kpc) SW of the nucleus and were taken as part of GO-5369. They contain 1200 s of exposure in *F606W* each. Field S3 contains 4200 s of exposure in *F814W*, while S2 contains only 2100 s in *F814W*.

### 2.2. Reduction

The data reduction and photometry for the ANGST survey are fully described in Dalcanton et al. (2009). For convenience, we provide a brief summary of the techniques here.

The photometry was simultaneously measured for all of the objects in the uncombined images using the software package HSTPHOT (Dolphin 2000). This package is optimized for measuring photometry of stars on WFPC2 images using the well-characterized and stable point spread function (PSF) calculated with TinyTim.<sup>6</sup> The software fits the PSF to all of the stars in each individual frame to find PSF magnitudes. It then determines and applies the aperture correction for each image using the most isolated stars, corrects for the charge transfer efficiency of the WFPC2 detector,<sup>7</sup> combines the results from the individual exposures, and converts the measured count rates to the VEGAMag system.

The HSTPHOT output was then filtered to only allow objects classified as stars with signal-to-noise ratio (total counts from the star to total noise)  $>4$  in both filters. The list was further culled using sharpness ( $|F606W_{\text{sharp}} + F814W_{\text{sharp}}| < 0.27$ ) and

<sup>6</sup> <http://www.stsci.edu/software/tinytim/>

<sup>7</sup> 2008 July formulae, [http://purcell.as.arizona.edu/wfpc2\\_calib/2008\\_07\\_19.html](http://purcell.as.arizona.edu/wfpc2_calib/2008_07_19.html).

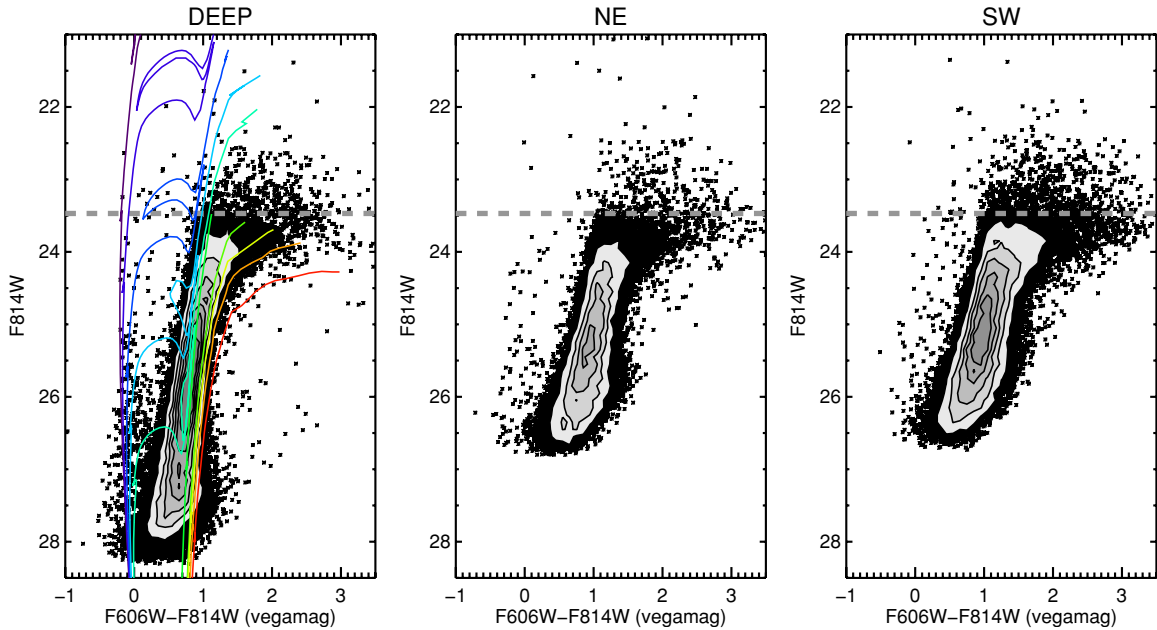


**Figure 2.** CMDs of our three WFPC2 fields (Section 2.2). Contours denote the density of points in areas of the plot that would otherwise be saturated. Overlaid on the deep field CMD are example isochrones from the Girardi et al. (2002) models shifted to  $m - M_0 = 27.48$ ,  $A_V = 0.08$  (from blue to red:  $[M/H] = -0.4$  and  $\log(\text{age}) = 7.3, 7.6, 8.0, 8.3, 8.6$ , followed by  $\log(\text{age}) = 10.0$  and  $[M/H] = -1.3, -0.7, -0.4, -0.2, 0.0$ , respectively). A gray-dashed line marks the TRGB as measured by Dalcanton et al. (2009).

(A color version of this figure is available in the online journal.)

crowding ( $F606W_{\text{crowd}} + F814W_{\text{crowd}} < 0.7$ ). The sharpness cut was chosen based on the distribution of values in the original catalog. The crowding parameter gives the difference between the magnitude of a star measured before and after subtracting the neighboring stars in the image. When this value is large, it suggests that the star's photometry was significantly affected by crowding, and we therefore exclude it from our catalog. Quality cuts based on the  $\chi$  values were also considered, but they were rejected when a correlation was found between  $\chi$  and the local background. Our final star catalogs contained 40793, 22332, and 33365 stars for the deep, NE, and SW fields, respectively. The archival outer disk fields S2 and S3 are much more sparsely populated. We obtained reliable photometry for only 468 and 692 stars for S2 and S3, respectively. The final CMDs for the fields are shown in Figures 2 and 3.

### 2.3. CMD Fitting

We measured the star formation rate and metallicity as a function of stellar age using the software package MATCH (Dolphin 2002). We fit the observed CMDs (with magnitude cuts set to limits provided in Table 1) by populating the stellar evolution models of Girardi et al. (2002, with updates in Marigo et al. 2008) with a Salpeter (1955) initial mass function (IMF) for a grid of assumed distance and foreground extinction values to allow for systematic differences in stellar evolution models and/or systematic photometric errors. The choices of software and models used for the ANGST project are discussed in detail in Williams et al. (2009a) and summarized in Dalcanton et al. (2009).

The best fits provide the combination of ages and metallicities that are contained in the observed field. We attempted to fit the data with a spread in the model photometry along the reddening line to account for the effects of differential reddening. However, applying a spread in reddening of  $A_V = 0.5$  to the models degraded the quality of the CMD fits, showing that differential

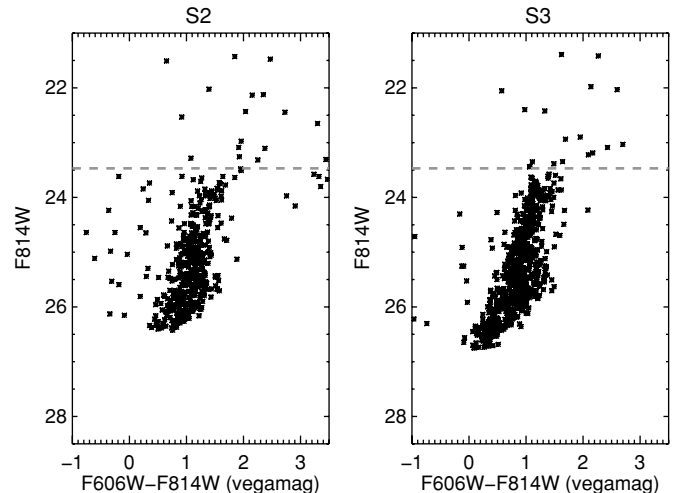


**Figure 3.** CMDs of the two archival WFPC2 fields in the outer disk (Section 2.2) previously studied by Tikhonov et al. (2003). A gray-dashed line marks the TRGB as measured by Dalcanton et al. (2009). We note the TRGB appears slightly fainter in these fields, explaining why the distance measurement of Tikhonov et al. (2003) was greater than that of Dalcanton et al. (2009).

reddening does not significantly affect our measurements in NGC 404.

The data from the deep field were best fit by a single foreground reddening  $A_V = 0.1 \pm 0.06$  and  $m - M_0 = 27.48 \pm 0.09$  (see Figure 4). This distance modulus is consistent with, but larger than, the value measured by the ANGST survey ( $m - M_0 = 27.42 \pm 0.02$ ; Dalcanton et al. 2009). The best-fit values compensate for any systematic differences between the data and overall model isochrones, whereas the survey value isolated the well-determined location of the tip of the red giant branch (TRGB) in order to measure the best distance. Since these distance and extinction values provided the best overall

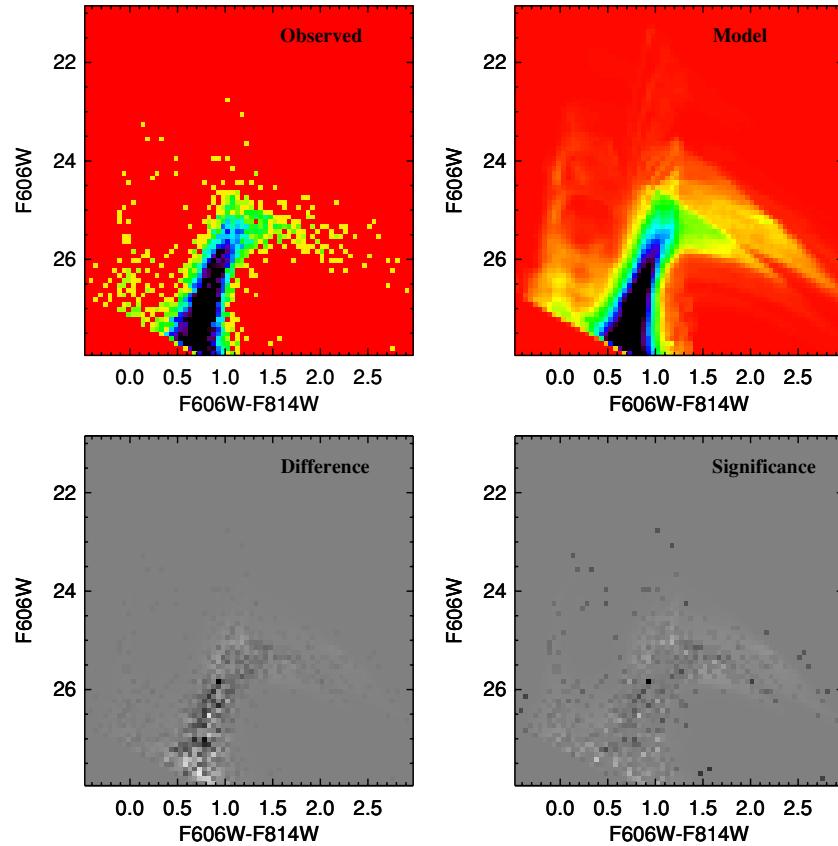


**Figure 4.** Our best-fit model CMD to the outermost annulus of the deep field data set (Section 2.3). This fit is our most reliable as it comes from our deepest photometry. Upper left: our observed CMD cut at the magnitude limits used for the fit. Upper right: best-fit model CMD. Lower left: difference between the data and the model. Darker colors denote excess stars in the data. Whiter colors denote excess stars in the model. The range is from  $-19$  (lightest) to  $+23$  (darkest), corresponding to fractional errors of  $\pm 0.5$ . Lower right: statistical significance of the residuals shown in lower left. The range is  $-5\sigma$  (lightest) to  $+10\sigma$  (darkest).

(A color version of this figure is available in the online journal.)

**Table 1**  
Properties of the Designated Regions

Region	$R_{\text{in}}$ (")	$R_{\text{out}}$ (")	$R_{\text{med}}$ (") <sup>a</sup>	$F_{606W_{50}}$ <sup>b</sup>	$F_{814W_{50}}$ <sup>c</sup>
Deep annulus 1	64.4	124.0	104.7	26.6	26.0
Deep annulus 2	124.0	160.0	142.1	27.3	26.3
Deep annulus 3	160.0	190.0	174.1	27.8	26.9
Deep annulus 4	190.0	268.4	215.1	28.0	27.2
NE annulus 1	93.0	124.0	111.9	26.8	25.8
NE annulus 2	124.0	160.0	140.9	26.9	26.1
NE annulus 3	160.0	190.0	173.0	27.0	26.1
NE annulus 4	190.0	250.5	208.3	27.2	26.3
SW annulus 1	64.0	124.0	95.2	26.6	25.8
SW annulus 2	124.0	160.0	136.8	26.9	26.0
SW annulus 3	160.0	190.0	168.7	26.9	26.2
S2	404.8	565.2	468.3	26.8	26.1
S3	406.7	560.6	480.8	26.9	26.4

**Notes.**

<sup>a</sup> The median galactocentric distance of the stars in the region.

<sup>b</sup> The 50% completeness limit of the  $F_{606W}$  data.

<sup>c</sup> The 50% completeness limit of the  $F_{814W}$  data.

fit of the models to the deepest data, we performed our fits to the data of every region assuming these values. Our systematic uncertainties in star formation rate account for changes in the SFH measured if the assumed value for the distance modulus was  $\pm 0.15$  mag away from the chosen value and if the extinction value was  $\pm 0.1$  mag away from the chosen value.

We note that in Figure 3 the apparent magnitude of the TRGB appears fainter than in our more populous CMDs. Our

fits to these CMDs (Figure 5) were not significantly improved by allowing a greater distance modulus, indicating that the small numbers of stars in these fields cause the TRGB to be under-populated. On the other hand, the SFHs of these fields could be significantly different than the inner fields. The shallow depth and low numbers of stars in these fields limit our ability to constrain the age. Our fits only show that 99% of the stars are older than 1.6 Gyr. Thus, it is possible that most of these stars are only a few gigayear old, which could produce a fainter TRGB. Unfortunately, there is not enough data to constrain whether the cause is undersampling or age. The CMD can be equivalently well-fitted by either possibility.

Systematic errors are determined by the MATCH package by comparing the results of SFHs from fits to the data with different values for the distance and foreground reddening to the field. These errors are then added in quadrature to the random errors governed by our sampling of the CMD. The random errors are determined by randomly drawing from the observed CMD to produce Hess diagrams that vary due to the Poisson statistics of our photometric sample. By producing and fitting 100 of these Monte Carlo CMDs, we are able to determine the rms of the residuals between SFHs from these fits and those from the fits to the original data. The combined  $1\sigma$  error measurements therefore account for the uncertainties in the distance to the galaxy, the foreground reddening, any systematic shifts between the model colors and magnitudes and our measured photometry, as well as the number of stars and features present in our CMD.

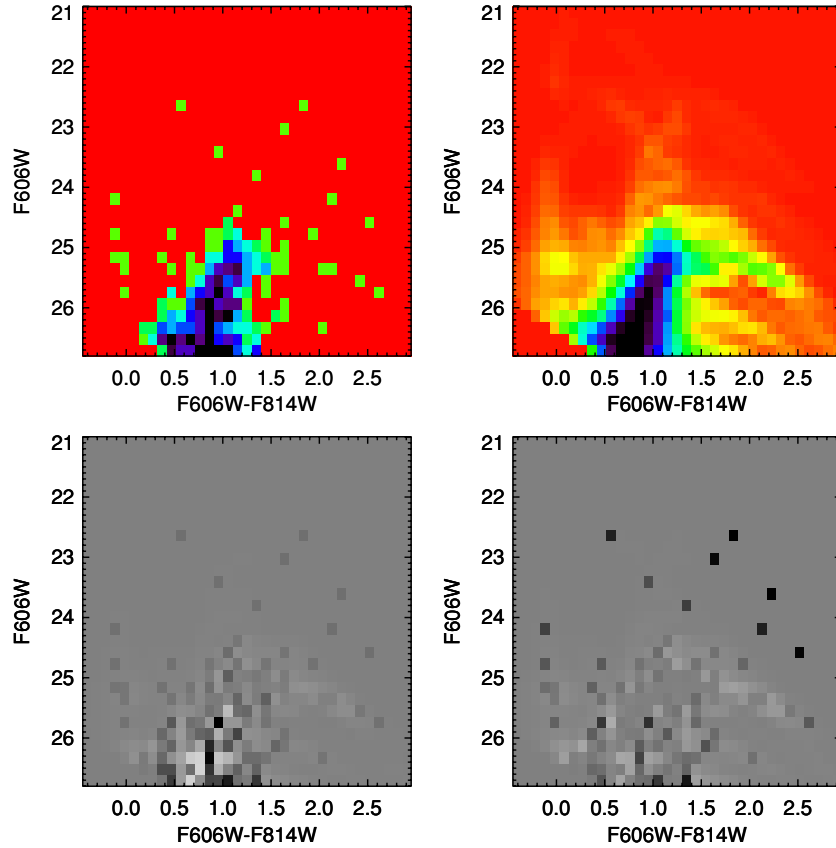


**Figure 5.** Our best-fit model CMD to the deeper of the two outer fields (S3). Panels are the same as Figure 4. The range is from  $-5$  (lightest) to  $+8$  (darkest), corresponding to fractional errors of  $^{+0.4}_{-0.6}$ . Lower right: statistical significance of the residuals shown in lower left. The range is  $-1.5\sigma$  (lightest) to  $+4.2\sigma$  (darkest). (A color version of this figure is available in the online journal.)

Our Monte Carlo tests are also used to determine our time sensitivity (i.e., the dependence of our SFH on our choice of time binning; see Williams et al. 2009b, for a full description of the technique). Briefly, we calculate the standard deviation of the maximum likelihood value from our 100 runs. We assume that any fit to the data more than one standard deviation away from the best fit is unacceptable. We then rerun our fits while suppressing star formation in various time bins. If the fit quality does not change significantly (by more than one standard deviation), we continue to expand the length of these removed time bins until the software can no longer find an acceptable fit. At this time resolution, we can be confident that our data provide meaningful constraints on the SFH. The final time bins are all sensitive enough that their removal from the SFH results in an unacceptable CMD fit.

#### 2.4. Depth

Photometric depth determines the precision with which we can recover the SFH of a region. The effects of age and metallicity are more difficult to distinguish with shallow photometry than with deep photometry. Our deepest photometry comes from our deep field and reaches the red clump in the least crowded region. This photometry therefore provides the most leverage for breaking the degeneracy between the age and metallicity of the old populations. In contrast, the data from our two shallow fields provide the least of this leverage. However, since the stellar populations should be well mixed at ages  $\gg 1$  Gyr, we used the metallicity distribution for the old stars ( $>2$  Gyr) as determined from the fit to our full deep field to limit the range

of allowed metallicities at each age in the fits to the shallower data. When the free parameters used to fit the shallower data were limited, we found the resulting age distribution of the ancient populations of the shallower fields to be consistent with those of the deep data, and the quality of the fit remained in the acceptable range (within one standard deviation of the value obtained when the full grid of free parameters was allowed). In what follows, the full-field SFHs for the shallower fields are the best fits possible with the restriction that the ancient population ( $>2$  Gyr) contain only the metallicities at each age that contributed to the best fit of the deep full-field data.

#### 2.5. Field Division

In addition to the full-field CMDs, we divided our inner disk fields into four annuli to look for radial trends of the stellar populations and to help minimize differential crowding effects across each field. The annuli were chosen so that each region contained  $\sim 10,000$  stars in our deep field data. The parameters of the annuli are provided in Table 1. Figure 6 shows the CMDs of the different annuli in our deep field. These CMDs clearly show that crowding in the inner regions is significantly worse than in the outer regions of our fields (as shown by the limited depth of photometry in the inner fields). In order to constrain the old populations of the two inner annuli, we limited the number of free parameters by allowing only the metallicities that provided the best fit to the outermost annulus of the deep field for ages  $>2$  Gyr. This restriction produced acceptable fits to the CMDs while forcing the ancient population of the innermost regions to be of similar metallicity to that of the outermost region.

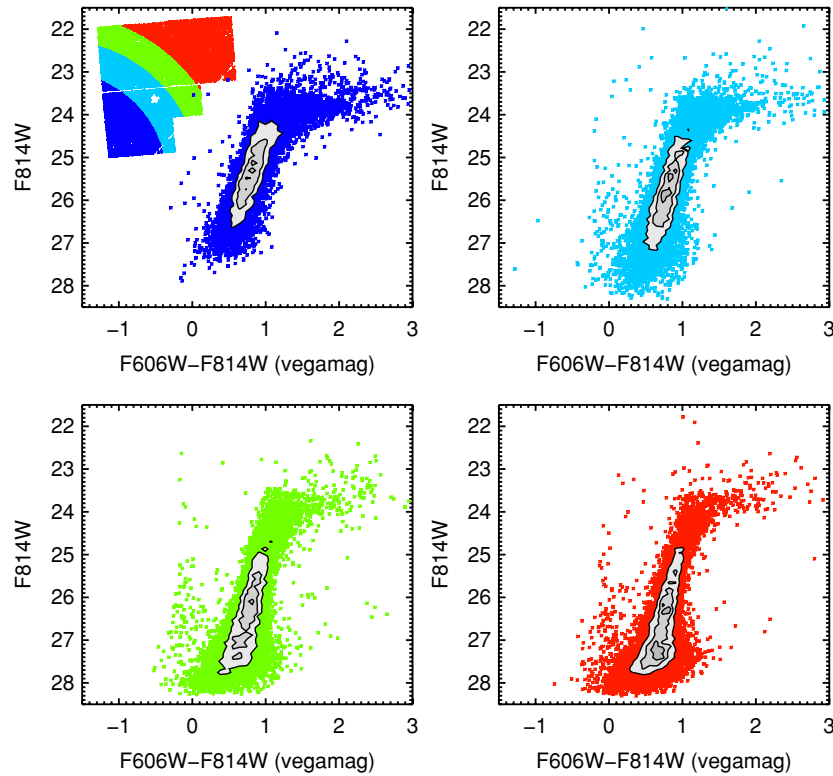


**Figure 6.** CMDs of the four annuli we defined for studying radial variations in the stellar populations (Section 2.5). The inset of the upper-left CMD shows the locations of the stars in each annulus on our deep WFPC2 field. Annuli were chosen to contain  $\sim 10,000$  stars each in the deep field. Radii of the boundaries are  $64''$ ,  $124''$ ,  $160''$ ,  $190''$ , and  $300''$ .

(A color version of this figure is available in the online journal.)

### 2.6. Spheroid Contamination

Baggett et al. (1998) performed an early bulge-disk decomposition on NGC 404 from digitized photographic plate observations in the  $V$  band, finding a bulge effective radius of  $63''.8$  and a disk scale length of  $129''.5$ . Their parameters indicate that the disk population is responsible for 50% of the galaxy light at  $\sim 165''$  (near the inner boundary of our third annulus from the center). Adopting this decomposition, our data are centered around the transition region between the domination of the bulge component and the domination of the disk component, suggesting our two outer annuli probe regions that are dominated by the disk population. However, more recently, the light profile of the bulge was measured with *HST* data, and the resulting effective radius was found to be smaller ( $38''$ ; Seth et al. 2010). We performed our own fit to the light profile using the *Spitzer*  $3.6 \mu\text{m}$  image from the local volume legacy (LVL) survey<sup>8</sup> for the central portions and normalizing to the star counts from our *HST* data. We found a similar effective radius ( $42''$ ). Our fit requires that 75% of the stars belong to the disk at  $165''$ . These measurements suggest that the amount of spheroid contamination inferred from the Baggett et al. (1998) decomposition is an upper limit, and all of our data are dominated by disk stars.

## 3. RESULTS

### 3.1. The Ancient Stellar Population of the Disk

The SFHs for our three fields are shown in Figure 7 (SFR versus time) and Figure 8 (the cumulative fractional star formation versus time). The SFH of the outer disk (archival fields

S2 and S3) was not well constrained due to the small number of stars. We note only that the weak constraints obtained from these fields ( $>98\%$  of the stellar mass formed before 1.6 Gyr ago) were consistent with the age distributions of the stars in the outer disk being the same as those in our three inner disk fields.

The stellar populations are clearly dominated by stars formed prior to 10 Gyr ago in all three fields. The cumulative age distribution of all of the fields is consistent with  $\gtrsim 70\%$  of the stellar mass formed by  $z \sim 2$ . Most of this constraint comes from the deep data, which provided the metallicity constraints for the shallower fields and has the greatest fraction of stellar mass formed prior to 10 Gyr. This initial star formation was then followed by roughly continuous star formation at low levels to very recent times ( $\lesssim 10$  Myr ago). *Galaxy Evolution Explorer* (*GALEX*) ultraviolet imaging is consistent with this low level of star formation continuing through the past few megayears and possibly to the present day (Thilker et al. 2010). The low recent star formation rate is consistent with the low surface density of H I ( $\sim 1.2 M_{\odot} \text{pc}^{-2}$ ; del R o et al. 2004). Such low-level extended star formation appears to be fairly common in moderately massive early-type galaxies as well as in some low-mass ones like NGC 404 (Salin & Rich 2010).

Our results show that the stars in our disk fields are older than any other disks previously studied in this manner; however, it is not clear if all parts of our fields are uniformly old. To address this question, we measured the SFH of our radial annuli. The cumulative SFHs of the stars in each of the four annuli are shown in Figures 9 and 10. These SFHs do not generally constrain the older populations as well as the full-field fits because the CMDs contain fewer stars. However, they are all consistent with  $\gtrsim 70\%$  of the stellar mass being formed by  $z \sim 2$ . The deepest

<sup>8</sup> <http://irsa.ipac.caltech.edu/data/SPITZER/LVL/>

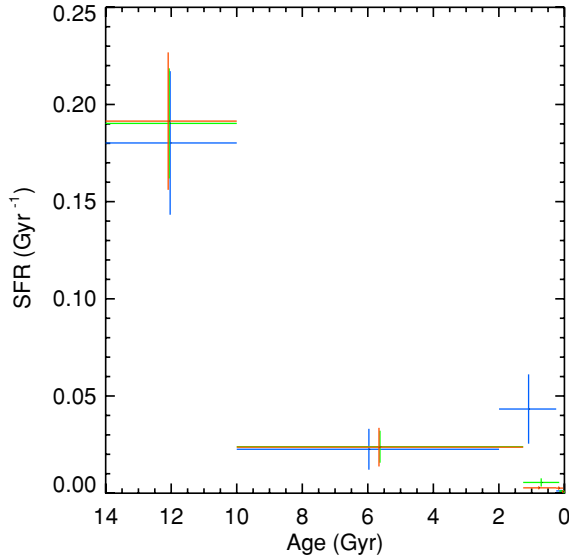


**Figure 7.** SFH of our three fields, normalized by total stellar mass in the field. This normalization produces units of fraction of the total field stellar mass produced each Gyr ( $\text{Gyr}^{-1}$ ). Blue, green, and red correspond to the results from the deep, SW, and NE fields, respectively. The units can be converted to  $M_{\odot} \text{yr}^{-1} \text{kpc}^{-2}$  by multiplying the  $\text{Gyr}^{-1}$  values by 0.038, 0.080, and 0.038, respectively. The SFHs of all fields agree and show most of the star formation occurring before 10 Gyr ago (Section 3.1).

(A color version of this figure is available in the online journal.)

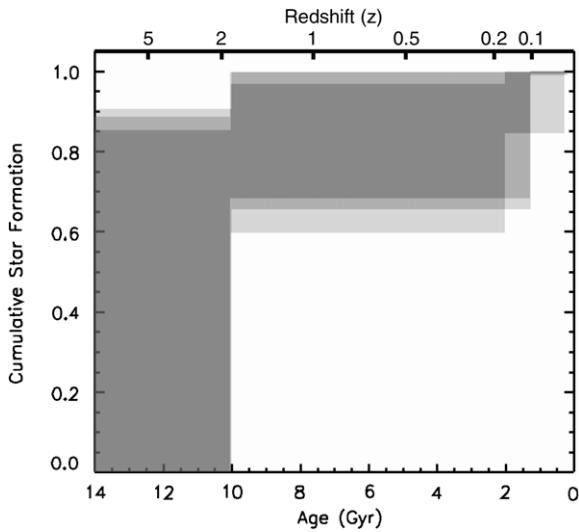


**Figure 8.** Cumulative SFH of our three fields. The results from each individual field are shaded in light gray. Areas of overlap between the SFH of different fields are darker. The darkest gray denotes the SFH that agrees with all of the fields. The results from all fields overlap significantly and suggest a disk dominated by very old ( $\gtrsim 10$  Gyr) stars (Section 3.1).

photometry in our sample, which comes from the outermost annulus of the deep field, constrains  $\gtrsim 90\%$  of the stellar mass to be older than 8 Gyr ( $z \sim 1$ ). The result from the outermost annulus of the shallower NE field is consistent with that result but does not provide nearly as tight of a constraint ( $>70\%$  of the stellar mass older than 2 Gyr) due to the lack of any of the red clump feature in the CMD. In the end, the SFHs of our different annuli allow the possibility that the inner annuli are a few gigayears younger on average than the outer annuli; however, it is not clear whether this difference is due to bulge contamination, shallower photometry, or true differences in age.

Because the full SFH measurements in our radial annuli did not show any conclusive differences between the stellar popu-

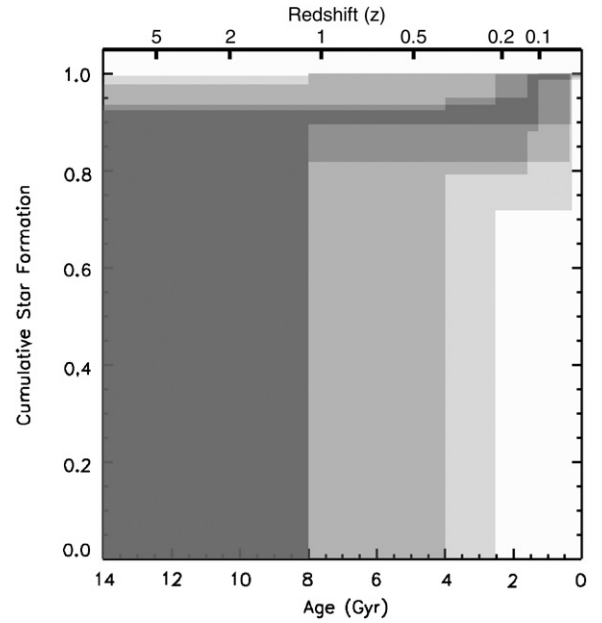


**Figure 9.** Cumulative SFH of our four annuli in just the deep field. The results from each individual annulus are shaded in light gray. Areas of overlap between the SFH of different annuli are darker. The darkest gray denotes the SFH that agrees with all of the annuli. The results from all annuli overlap significantly, although the inner annuli do not provide as much constraint on the age distribution of stars older than 2 Gyr as the deeper outer annuli. The fact that the SFHs of all annuli overlap with that of the well-constrained outermost annulus suggests little radial variation of the stellar populations in the deep field (Section 3.1).

lations of the NGC 404 disk with radius, we attempted a more traditional method of comparing the asymptotic giant branch (AGB)/RGB ratios in different regions. Tikhonov et al. (2003) found that inside of  $r \sim 150''$ , the ratio of AGB to RGB stars decreases with radius, which they interpret as evidence for most of the AGB population being associated with the bulge. Our constraints on the detailed age distribution in the inner annuli allow the possibility that the inner regions are younger than the outer regions. Furthermore, our innermost annulus has a slightly bluer RGB and a higher AGB/RGB ratio than the other annuli studied, consistent with the Tikhonov et al. (2003) results. Gaussian fits to a slice through the CMDs in Figure 6 at  $m_{F814W} = 24.75$  give a central RGB color of  $m_{F606W} - m_{F814W} = 0.95 \pm 0.01$  in our innermost annulus, while those of the outer annuli and outer disk fields are all  $\geq 0.98$ . The ratio of AGB stars ( $m_{F814W} < 23.5$ ) to RGB stars ( $25.0 > m_{F814W} > 23.5$ ) is  $0.056 \pm 0.005$  in the innermost annulus, while those of the outer annuli are all  $< 0.05$ . This ratio was not reliably constrained in the outer disk fields (S2 and S3), due to the low numbers of stars. Overall, the results of our full CMD fitting, as well as direct measurements of our CMDs' features, are consistent with the suggestion in Tikhonov et al. (2003) that NGC 404 contains a bulge population that is on average *younger* than the disk. However, with the current data we cannot distinguish between this possibility and the possibility of radial variations in the mean age of the disk itself.

The metallicity history from our deep field is shown in Figure 11. As with many other nearby galaxies, we find that NGC 404 quickly enriched to  $[M/H] \gtrsim -1$  and then appears to have undergone more modest subsequent chemical enrichment. The errors are very large on the metallicity of the young populations both because the number of young stars is low and because the properties of the upper-main sequence is not

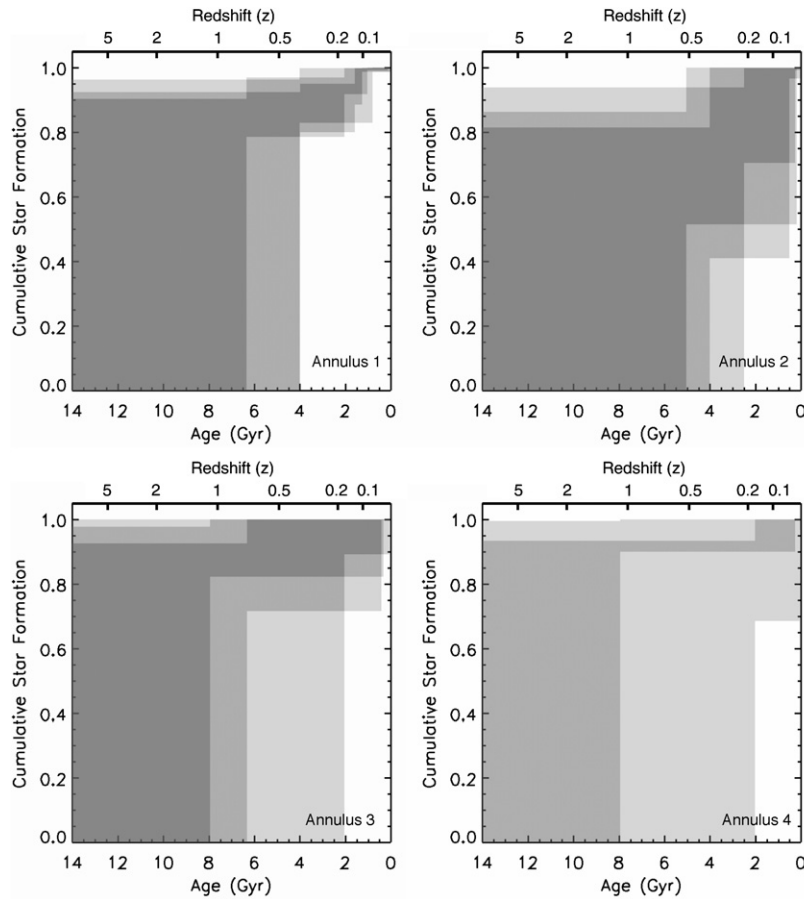


**Figure 10.** Cumulative SFH of our four annuli. The results from each field are shaded in light gray. Areas of overlap between the SFH of the same annulus in different fields are darker. The darkest gray denotes the SFH that agrees with all of the data. The results from all fields overlap significantly, but the deep field constrains the stellar populations to be dominated by the oldest stars (Section 3.1).

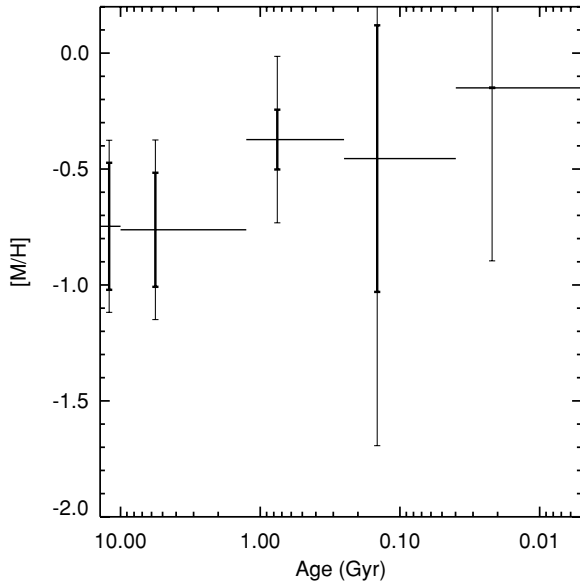


**Figure 11.** Chemical enrichment history of NGC 404 from our CMD fit to the deep field. Thick error bars mark the spread in metallicity, while thin error bars show the estimated uncertainty in the mean metallicity and spread. The ancient stars are dominated by metallicities  $> -1.0$ , and there is evidence of an increase at times more recent than  $\sim 1$  Gyr ago (Section 3.1).

strongly affected by metallicity. Therefore, while our metallicity history does not show any obvious discontinuities, if recently accreted gas was of different metallicity than the previously

existing gas disk, it is not clear we would have detected the difference with statistical significance. Indeed, the allowed metallicity range in the 30–300 Myr time bin allows any metallicity  $[M/H] \geq -1.7$ .

From these results, we can assign the typical age and metallicity of the stars in these portions of NGC 404 as  $12 \pm 2$  Gyr and  $-0.75 \pm 0.37$ . These values are consistent with those determined from fits to optical spectra of the bulge ( $>50\%$  of the stars  $> 5$  Gyr old and  $[M/H] \sim -0.4$ ; Seth et al. 2010), indicating overall similarity between the bulge and disk populations in NGC 404, partially explaining the lack of radial trends in our SFHs.

The typical age and metallicity of the stars in NGC 404 can be compared to those of other nearby galaxies, as was done in Williams et al. (2009a). This comparison is shown in Figure 12. It shows the NGC 404 disk fields have the oldest typical age of any disk fields in the nearby sample; however, the age was determined closer to the galaxy center than for any of the other galaxies. Note that the two oldest populations, those of the Galactic thick disk and NGC 404, are those measured closest to the galaxy centers.

### 3.2. The Young Stellar Population

Although the star formation in NGC 404 over the past gigayear amounts to an insignificant fraction of the stellar mass of the disk, it is of interest for understanding any radial trends in star formation activity as well as the origin of gas in the NGC 404 disk and its likely fate. We show the most recent gigayear of

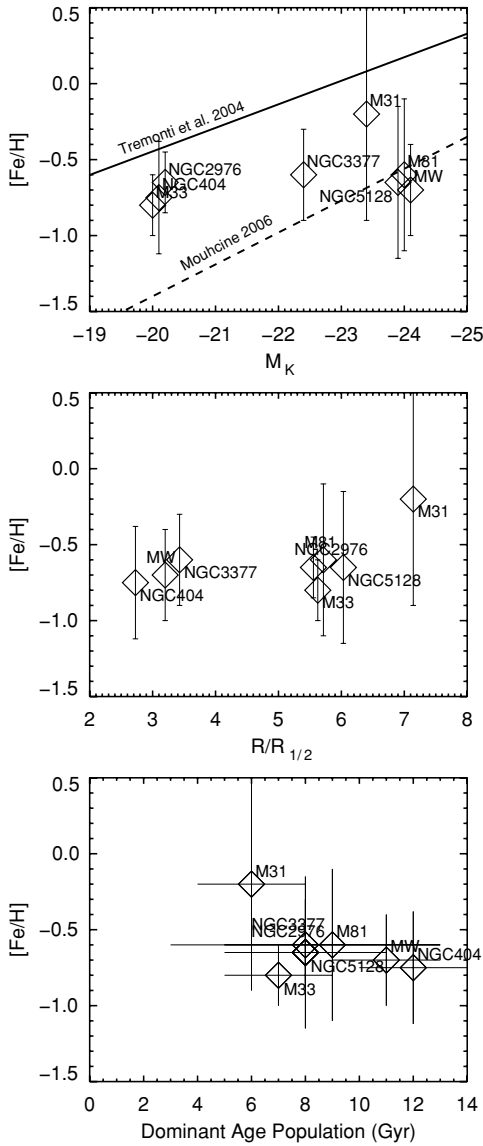


**Figure 12.** Metallicity range of the dominant stellar populations in deep resolved photometry for M31 (Brown et al. 2006), M33 (Barker et al. 2007), M81 (Williams et al. 2009a), NGC 5128 (Rejkuba et al. 2005), NGC 3377 (Harris et al. 2007), NGC 2976 (Williams et al. 2009b), and NGC 404 (this work) are plotted along with that of the Milky Way thick disk (Allende Prieto et al. 2006) against several other properties (Section 3.1). Top: metallicities as a function of the absolute  $K$ -band magnitude of the galaxy (Skrutskie et al. 2006). The solid and dashed lines show the luminosity–metallicity relations determined by Tremonti et al. (2004, gas phase metallicity) and Mouhcine (2006, stellar red peak metallicities of galaxy “halos”), respectively. These relations were converted from  $B$  band and  $V$  band to  $K$  band using the Tully–Fisher calibrations of Verheijen (2001) and Sakai et al. (2000). The Milky Way luminosity was calculated by applying  $V_{\text{rot}} = 220 \text{ km s}^{-1}$  to the Tully–Fisher calibration of Verheijen (2001). Middle: populations’ metallicities as a function of the radii at which they were sampled (normalized to the half-light radius of the galaxy). Bottom: populations’ metallicities as a function of their ages.

the SFHs of the full fields in Figure 13, along with the weighted average of all star formation in all fields. We show these results at a higher time resolution ( $\sim 200 \text{ Myr}$ ), since our time resolution is good at these ages due to the rapidly evolving bright main- and blue He burning sequences, which contain information for ages  $\lesssim 500 \text{ Myr}$ . For the outer disk fields, we were not able to reliably determine ages from 400 to 1000 Myr, due to the small numbers of stars in these fields. We therefore limited the age range to just two time bins for those fields.

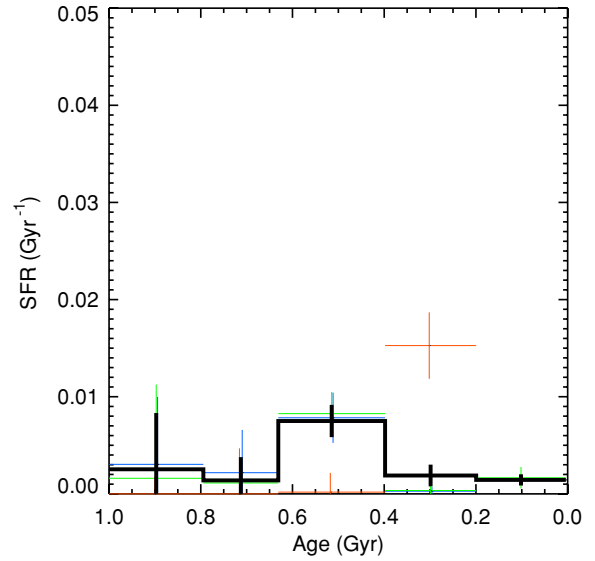


**Figure 13.** Colored error bars: recent star formation histories of the three fields. Colors, normalization, and units are the same as in Figure 7. Black histogram: combination of all of the SFHs of the individual regions. The combination shows a significant increase in the star formation rate  $\sim 500 \text{ Myr}$  ago (Section 3.2). (A color version of this figure is available in the online journal.)

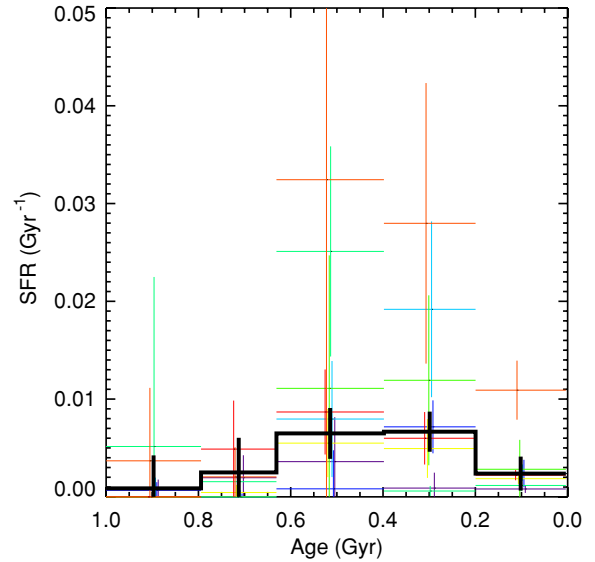


**Figure 14.** Colored error bars: recent star formation histories of all of the annuli outside of the innermost, normalized by total stellar mass in the field. This normalization produces units of fraction of the total field stellar mass produced each Gyr ( $\text{Gyr}^{-1}$ ). Black histogram: combination of all of the SFHs of the individual regions. The combination shows a significant increase in the star formation rate  $\sim 500 \text{ Myr}$  ago (Section 3.2). The combined values can be converted from  $\text{Gyr}^{-1}$  to  $M_{\odot} \text{ yr}^{-1} \text{ kpc}^{-2}$  by multiplying the  $\text{Gyr}^{-1}$  values by 0.033.

(A color version of this figure is available in the online journal.)

There do not appear to be any radial trends nor any strong positional dependencies of the recent SFH in the our NGC 404 disk fields (see discussion below). However, a distinct pattern emerges in the global SFHs of the full fields as well as all of the annuli beyond the innermost (and shallowest) one. The pattern is plotted in Figures 13 and 14, which show all of the recent SFHs in color and their mean in black. The best fits to all fields suggest that star formation substantially increased  $\sim 500 \text{ Myr}$  ago, rising from consistent with zero to

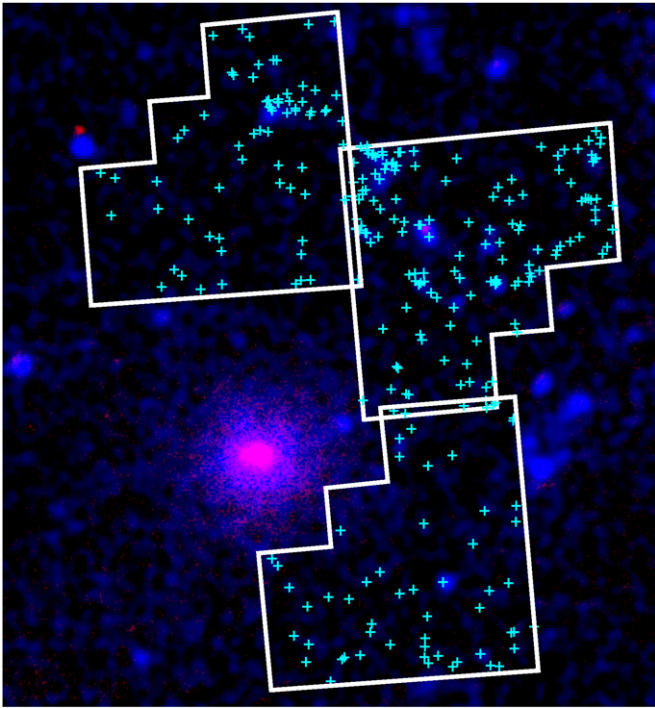


**Figure 15.** Locations of the upper-main-sequence stars from our *HST* images (cyan crosses) are shown on a composite *GALEX* far-UV (blue),  $H\alpha$  (red) image (Section 3.2). All the FUV-bright regions contain these young stars, but the young stars are not confined to the FUV-bright regions. Also note the very low amount of  $H\alpha$  emission present.

$\sim 2 \times 10^{-4} M_{\odot} \text{ yr}^{-1} \text{ kpc}^{-2}$  by  $\sim 400$  Myr ago, but then falling to a lower level by the present. Indeed, no star formation is required during the interval 1.3–0.3 Gyr ago to produce statistically acceptable fits to the CMD of the deep field; likewise, no star formation is required during the interval 2–0.3 Gyr ago to fit the NE field and during the interval 1.3–0.2 Gyr ago to fit the SW field. Likewise, no star formation more recent than  $\sim 100$  Myr ago is required to fit the CMDs of any of the fields either, showing that any very recent ( $< 100$  Myr) star formation has been at a very low level, consistent with the lack of any diffuse  $H\alpha$  emission (Figure 15). Thus, all of our measurements (outside of the innermost annulus) require star formation in the past few hundred megayears. While our data allow the possibility that this star formation was confined to the past 300 Myr, the best fits to our data have this star formation confined mainly to a small event that occurred  $\sim 600$ –200 Myr ago.

The recent SFHs from the outer disk data (archival fields S2 and S3, Figure 16) are consistent with those obtained from the inner disk after scaling by stellar density. However, we were unable to reliably constrain the age distribution earlier than 400 Myr ago due to the shallow depth and small number of stars in these fields, which are located  $\sim 2.3$  scale lengths ( $r_s = 129''$ ; Baggett et al. 1998) farther out in the disk. The best fits to the outer disk fields suggest an increase in star formation beginning at a similar time ( $\sim 400$  Myr ago) as seen in the inner disk fields, with an intensity that is a factor of 10 less than in the inner disk fields, consistent with a simple density scaling.

To look for variations in the most recent ( $\lesssim 160$  Myr) star formation with position in our inner disk fields, we computed the mass of stars formed in all 11 of our defined regions (4 annuli each in the deep and NE fields, and 3 annuli in the SW field) during the past 160 Myr according to our measured SFHs. This age range probes all O- and early B-type stars, and thus

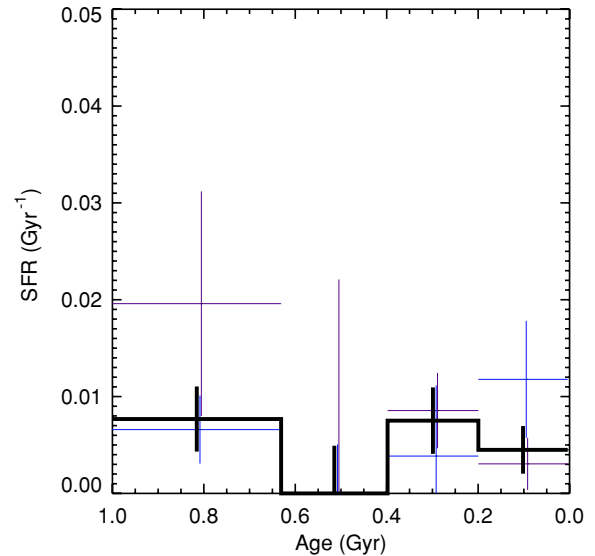


**Figure 16.** Colored error bars: recent star formation histories of the two outer disk fields, normalized by total stellar mass in the field. This normalization produces units of fraction of the total field stellar mass produced each Gyr ( $\text{Gyr}^{-1}$ ). Black histogram: combination of the SFHs of the two outer disk fields. The SFH is consistent with an increase in star formation beginning  $\sim 400$  Myr ago, and the star formation rate over the past 400 Myr is consistent with a simple scaling of the rate in the inner disk fields with density (Section 3.2).

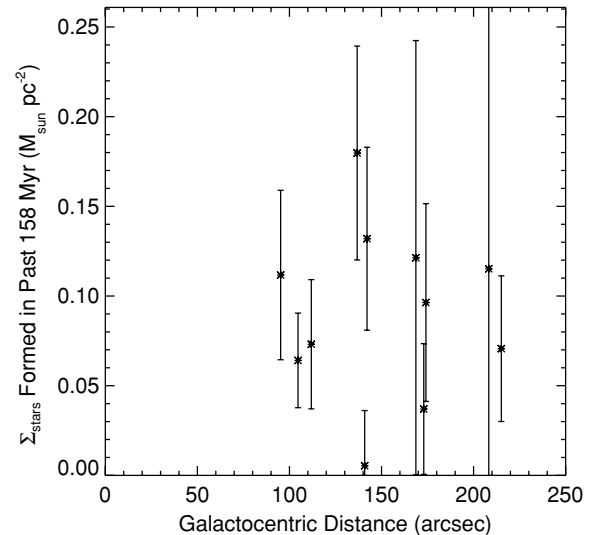


**Figure 17.** Surface density of stars formed in the past 158 Myr as a function of galactocentric distance in the NGC 404 disk. No trend with radius is apparent (Section 3.2).

provides a good baseline for comparison with the FUV fluxes measured from the *GALEX* data.

We plot the median radius of the stars in each of our regions versus the mass of stars formed in the past 158 Myr in Figure 17. No radial trend is seen, suggesting that, overall, the recent SFH of the disk has not been a strong function of radius in the inner ( $< 5$  kpc) disk, and is more consistent with star formation percolating stochastically across the face of the inner disk (McQuinn et al. 2009). These results suggest that there is little, if any, change in the young disk stellar populations with galactocentric distance in NGC 404 from 1 to 9 arcmin, which covers  $\sim 3.7$  scale lengths of the disk and  $\sim 9$  effective radii.

We have further tested our ability to detect the star formation responsible for the flux in the *GALEX* FUV image, which

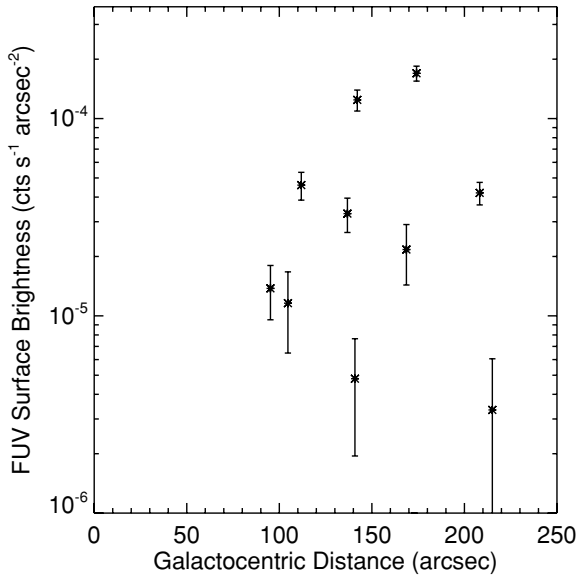


**Figure 18.** *GALEX* FUV surface brightness as a function of galactocentric distance in the NGC 404 disk. No trend with radius is apparent (Section 3.2).

appears as discrete knots of star formation in the NGC 404 disk (see Figure 1). We first measured the FUV luminosity of these knots in each of our defined regions (see Figure 1) using SExtractor (Bertin & Arnouts 1996). We then subtracted the expected foreground/background luminosity as determined from a control region 10 scale lengths from the galaxy center. We find that the FUV luminosity does not correlate with galactocentric distance (see Figure 18), which is consistent with our result that the amount of recent ( $\lesssim 160$  Myr) star formation does not correlate with galactocentric distance (other than simply scaling with density). On the other hand, there is a hint of a correlation between the FUV luminosity of the knots and the mass of stars formed in the past 160 Myr, shown in Figure 19. A Spearman rank test reveals that a correlation is present at only the  $2\sigma$  level (5% probability of no correlation).

The fact that the correlation is weak may seem surprising, but the reason for the weakness is apparent when one looks at the mean age of the stars younger than 160 Myr in each region. The colors of the error bars in Figure 19 indicate this mean age, with redder colors representing older ages. With this additional information, it is clear that the most FUV-luminous regions contain the youngest stars, but not the highest stellar masses. At a given age (similar color points), the FUV luminosity correlates better with the stellar mass of young stars.

Such a scatter in age should be reflected in the FUV–NUV colors of the regions. We measured these colors and found  $\pm 0.8$  mag rms scatter. About 0.3 mag of scatter is expected from photometric errors as determined by photon statistics. Some of the additional scatter is due to the presence of foreground stars in the NUV. Varying extinction is not severe enough to explain any additional scatter. In the *GALEX* bandpasses,  $A_{\text{FUV}}/E_{(B-V)} = 8.376$  and  $A_{\text{NUV}}/E_{(B-V)} = 8.741$  (Wyder et al. 2005), or  $E_{(\text{FUV-NUV})}/E_{B-V} = -0.365$ . Thus, the scatter in  $E_{(B-V)}$  needed to explain the measured scatter in FUV–NUV is  $\pm 2.2$  mag. Such a large amount of differential extinction would be far more than we observe in our CMDs. While we cannot easily quantify the effects of foreground contamination, the scatter in FUV–NUV color supports the idea that a range of ages is in large part responsible for the weakness of the correlation.

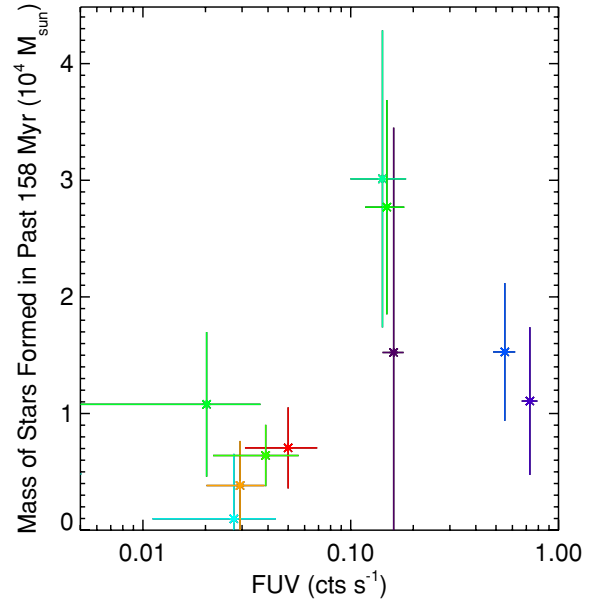


**Figure 19.** Total stellar mass formed in the past 158 Myr as a function of total *GALEX* FUV flux measured in the regions shown in Figure 1, defined by the WFPC2 field edges and radial annuli. Redder colors denote higher mean ages for the stars formed in the past 158 Myr. Only a slightly significant trend is seen, partially due to the differences in the mean age of the young stellar mass in the different regions (Section 3.2).

Furthermore, the distribution of upper-main-sequence stars on the *GALEX* FUV image, shown in Figure 15, suggests that these young stars are more widely distributed than the FUV emission. While all FUV-bright regions contain upper-main-sequence stars, not all upper-main-sequence stars are confined within FUV-bright regions. The different distributions could be explained by stars migrating away from their birth regions on timescales  $< 160$  Myr (consistent with Lada & Lada 2003), and FUV emission being dominated by stars younger than 100 Myr (consistent with Gogarten et al. 2009). These results show that there is a complex relationship between UV properties, age, and stellar mass in regions containing recent star formation.

### 3.3. The Origin of the Gas Disk

It is interesting that our SFHs show an increase in star formation  $\sim 0.5$  Myr ago, in the light of the suggestion of del Río et al. (2004) that the gas disk may have originated in a merger event with a dIrr galaxy 0.5–1 Gyr ago. However, our full-field CMDs all require some star formation between 2 and 10 Gyr, as well as star formation between 0.5 and 0.1 Gyr ago, to produce an acceptable fit to the observed CMD. Failure to include stars in the 2–10 Gyr age range produces a model CMD containing more blue AGB stars above the RGB tip than are seen in the data. These stars produce a quantitatively significant decrease in the quality of the model fit. The lower limits on the star formation rates in the 2–10 Gyr period are comparable to the peak rates over the past 500 Myr.

To investigate the origin of the gas in the disk, we studied the correlation between gas density and star formation in the disk of NGC 404 over its history. We assume that all of the stars that formed during a given time interval in our SFH must have been in the form of gas at the beginning of that time interval. When this gas is added to the gas seen at the present day, we can infer the gas density in the past, and then compare it to the subsequent star formation rate in our SFH. We can do this at increasing

look-back times, giving us a way of probing the correlation between gas density and star formation rate at a range of epochs.

We begin with the current H I column density of the disk from  $2' - 5'$  ( $\sim 1.5 \times 10^{20} \text{ cm}^{-2}$ ; del R o et al. 2004), which corresponds to  $1.2 M_{\odot} \text{ pc}^{-2}$ . We then assume that  $\Sigma_{\text{H}} = \Sigma_{\text{H I}}$  and adopt the conversion  $\Sigma_{\text{gas}} = 1.45 \Sigma_{\text{H}}$  (Kennicutt 1989) to account for metals and molecular gas. Finally, we assume that all stars formed from a previously existing gas disk that was in place at the beginning of each time interval. Our method therefore requires that the gas disk had a higher surface density in the past in order to provide the material for all of the star formation that subsequently occurred. We further assume that stellar evolution quickly recycles 20% of the mass of stellar mass back to the gas phase. This fraction corresponds to all stars  $> 8 M_{\odot}$  (assuming a Kroupa IMF integrated from  $0.1 M_{\odot}$  to  $100 M_{\odot}$ ), which return their mass to the interstellar medium on timescales shorter than 100 Myr. The exact value of this fraction had minimal impact on our estimates.

With the above assumptions, we were able to infer the gas density of the disk for several epochs in the history of NGC 404 and compare that density to our measured star formation rates. We were then able to test the plausibility of the assumptions by comparing the results to the known correlation between gas density and star formation rate (Bigiel et al. 2008). The results of this reconstruction of the history of the gas density and star formation rate in the NGC 404 inner disk are shown in Figure 20, where diamonds show the gas density and mean star formation rates of the disk for each of five epochs (0.3, 0.6, 0.9, 5, 12 Gyr ago) calculated from our measured SFHs. The  $\Sigma_{\text{SFR}}$  versus  $\Sigma_{\text{gas}}$  in the early epochs agrees with the overall trends measured by the H I Nearby Galaxy Survey (THINGS; Bigiel et al. 2008) under the assumption that all of the stars formed from a gas disk that was formed  $\sim 14$  Gyr ago. However, at 0.9 Gyr, the star formation rate is inconsistent with the gas density under this ‘‘closed-box’’ assumption.

To test the possibility that a recent merger with a small gas-rich galaxy may have affected the evolution of the NGC 404 disk, we performed a reconstruction of the past gas density and star formation rate described above, but we altered the closed-box assumption. Instead, we assume that  $10^8 M_{\odot}$  of gas was added to the system 0.6–0.9 Gyr ago. The effect of this assumption is to make the gas density of the disk significantly lower  $\sim 1$  Gyr ago than it is today, unlike the closed-box assumption where the gas density strictly increases with look-back time. The triangle points with dotted errors in Figure 20 show the results of this reconstruction. These points, including the one at 0.9 Gyr, are all consistent with the known correlation between gas density and star formation rate. This consistency allows the possibility that gas was recently accreted, as was suggested by del R o et al. (2004) based on the warped nature of the outer gas disk.

Together, these results favor a scenario where a gas disk was in place for many gigayears. This disk was of low surface density ( $< 5 M_{\odot} \text{ pc}^{-2}$ ) for most of the history of the disk and formed stars at a low rate ( $< 10^{-3} M_{\odot} \text{ yr}^{-1} \text{ kpc}^{-2}$ ). This gas may have been completely depleted by  $\sim 1$  Gyr ago, when new gas entered the system, either from surrounding gas filaments, or from a small, gas-rich, dwarf galaxy that merged to produce the current gas disk. This event triggered a small amount of new star formation over the past  $\sim 500$  Myr.

It is still possible that the present gas disk is a relic of the gas that originally formed the disk and that there was no recent merger. If so, the low-density gas disk must have formed stars in short, weak, episodes that lasted  $\sim 200$ – $400$  Myr. Such episodes,

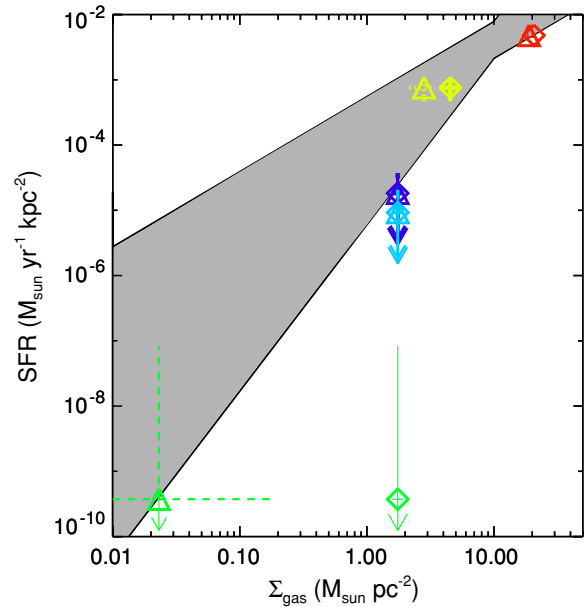


**Figure 20.** Diamonds with solid errors: gas surface density at previous epochs assuming all gas was in place 14 Gyr ago. Redder colors denote older ages (0.3, 0.6, 0.9, 5, 12 Gyr). Triangles with dotted errors: gas surface density at previous epochs assuming a gas accretion event occurred 0.6–0.9 Gyr ago. Colors are the same ages as the diamonds. Shaded area: regions of gas density–star formation rate density space covered by the relation measured by THINGS (Bigiel et al. 2008). Note that the star formation rate was far too low for the assumed gas density 0.9 Gyr ago, if we assume no gas has been accreted (light blue diamond; Section 3.3).

like the one we have resolved in the most recent Gyr, form only  $\lesssim 10^7 M_{\odot}$  of stellar mass in the inner disk ( $r < 5$  kpc, assuming axisymmetry), which could reconcile the amount of stars formed in the past gigayear with the amount of gas available in our closed-box assumption. Such star formation would be insignificant compared to the  $\gtrsim 2 \times 10^9 M_{\odot}$  of stellar mass formed in the inner disk prior to 10 Gyr ago and the  $1.5 \times 10^8 M_{\odot}$  of H I present (del R o et al. 2004). Such a scenario is favored by the isolated environment of NGC 404 but is not consistent with the star formation rates we measure from 0.6 to 1.0 Gyr. Furthermore, del R o et al. (2004) suggest the warped nature of the gas disk as additional evidence for the recent merger. While the warp is consistent with the merger scenario, warping can also occur from misalignment of angular momentum during late gas accretion from filaments (Jiang & Binney 1999; Shen & Sellwood 2006) and therefore does not require a catastrophic merger.

#### 4. CONCLUSIONS

We have measured resolved stellar photometry for  $\sim 15$  arcmin<sup>2</sup> of the inner disk and  $\sim 10$  arcmin<sup>2</sup> of the outer disk of the S0 galaxy NGC 404. Detailed fitting of the resulting CMDs shows that the disk is dominated by stars older than  $\sim 10$  Gyr, with all of our inner disk data constraining the age of  $\sim 90\%$  of the stellar mass to  $> 8$  Gyr and our best data constraining the age of 70% of the stellar mass to  $> 10$  Gyr. These results show that the difference between this disk and most later-type disks that have been studied in detail is seen in the old stellar population as well as the young.

We found no trends between the age distributions of the young or old populations and distance from the galaxy center within the observed regions. However, as seen by Tikhonov et al. (2003), the mean RGB color and AGB/RGB ratio of the innermost

regions are consistent with a bulge population in NGC 404 that is younger than the disk.

Despite its low gas density, NGC 404 appears to have been forming stars throughout its history on timescales of gigayear, even in the inner disk ( $\sim 1' - 1.5'$ ). The SFH and the current density of the gas disk are consistent with NGC 404 having evolved roughly in a closed box over much of its history, starting as a large disk of high surface density and approximately following the Schmidt law as its overall star formation rate and gas density decreased. Such long-lived disks have been observed in isolated galaxies before, as in the compact dwarf ADBS 113845+2008 (Cannon et al. 2009), whose gas disk is also of low density. Perhaps these low-density disks have very long lifetimes due to very low star formation efficiencies at these densities. Our SFHs indicate that star formation in the low-density relic disk may be episodic, going through minor episodes of star formation that last a few hundred megayears every gigayear or so.

On the other hand, in NGC 404, there is some evidence that this passive evolution was slightly disrupted by an event 0.6–0.9 Gyr ago, possibly a small merger. Such a merger event would alleviate the necessity for very low star formation efficiency  $\sim 1$  Gyr ago by allowing that the currently observed gas disk was not fully in place at that time.

Support for this work was provided by NASA through grants GO-10915 and GO-11719 from the Space Telescope Science Institute, which is operated by the Association of Universities for Research in Astronomy, Incorporated, under NASA contract NAS5-26555.

## REFERENCES

- Allende Prieto, C., Beers, T. C., Wilhelm, R., Newberg, H. J., Rockosi, C. M., Yanny, B., & Lee, Y. S. 2006, *ApJ*, 636, 804
- Baggett, W. E., Baggett, S. M., & Anderson, K. S. J. 1998, *AJ*, 116, 1626
- Barden, M., et al. 2005, *ApJ*, 635, 959
- Barker, M. K., Sarajedini, A., Geisler, D., Harding, P., & Schommer, R. 2007, *AJ*, 133, 1138
- Bertin, E., & Arnouts, S. 1996, *A&AS*, 117, 393
- Bigiel, F., Leroy, A., Walter, F., Brinks, E., de Blok, W. J. G., Madore, B., & Thornley, M. D. 2008, *AJ*, 136, 2846
- Bouchard, A., Prugniel, P., Koleva, M., & Sharina, M. 2010, *A&A*, 513, 54
- Brown, T. M., Smith, E., Ferguson, H. C., Rich, R. M., Guhathakurta, P., Renzini, A., Sweigart, A. V., & Kimble, R. A. 2006, *ApJ*, 652, 323
- Cannon, J. M., Salzer, J. J., & Rosenberg, J. L. 2009, *ApJ*, 696, 2104
- Dalcanton, J. J., et al. 2009, *ApJS*, 183, 67
- Davidge, T. J. 2008, *AJ*, 135, 1636
- del Río, M. S., Brinks, E., & Cepa, J. 2004, *AJ*, 128, 89
- Dolphin, A. E. 2000, *PASP*, 112, 1383
- Dolphin, A. E. 2002, *MNRAS*, 332, 91
- Dunkley, J., et al. 2009, *ApJS*, 180, 306
- Ford, H. C., et al. 1998, Proc. SPIE, 3356, 234
- Girardi, L., Bertelli, G., Bressan, A., Chiosi, C., Groenewegen, M. A. T., Marigo, P., Salasnich, B., & Weiss, A. 2002, *A&A*, 391, 195
- Gogarten, S. M., et al. 2009, *ApJ*, 691, 115
- Harris, W. E., Harris, G. L. H., Layden, A. C., & Stetson, P. B. 2007, *AJ*, 134, 43
- Jiang, I.-G., & Binney, J. 1999, *MNRAS*, 303, L7
- Karachentsev, I. D., Karachentseva, V. E., Huchtmeier, W. K., & Makarov, D. I. 2004, *AJ*, 127, 2031
- Kennicutt, R. C., Jr. 1989, *ApJ*, 344, 685
- Lada, C. J., & Lada, E. A. 2003, *ARA&A*, 41, 57
- Li, J.-T., Wang, Q. D., Li, Z., & Chen, Y. 2009, *ApJ*, 706, 693
- MacArthur, L. A., Courteau, S., Bell, E., & Holtzman, J. A. 2004, *ApJS*, 152, 175
- Maoz, D., Koratkar, A., Shields, J. C., Ho, L. C., Filippenko, A. V., & Sternberg, A. 1998, *AJ*, 116, 55
- Marigo, P., Girardi, L., Bressan, A., Groenewegen, M. A. T., Silva, L., & Granato, G. L. 2008, *A&A*, 482, 883
- McQuinn, K. B. W., Skillman, E. D., Cannon, J. M., Dalcanton, J. J., Dolphin, A., Stark, D., & Weisz, D. 2009, *ApJ*, 695, 561
- Melbourne, J., Phillips, A. C., Harker, J., Novak, G., Koo, D. C., & Faber, S. M. 2007, *ApJ*, 660, 81
- Mouhcine, M. 2006, *ApJ*, 652, 277
- Poggianti, B. M., et al. 2009, *ApJ*, 697, L137
- Pohlen, M., Balcells, M., Lütticke, R., & Dettmar, R.-J. 2004, *A&A*, 422, 465
- Ravindranath, S., et al. 2004, *ApJ*, 604, L9
- Rejkuba, M., Greggio, L., Harris, W. E., Harris, G. L. H., & Peng, E. W. 2005, *ApJ*, 631, 262
- Sakai, S., et al. 2000, *ApJ*, 529, 698
- Salim, S., & Rich, R. M. 2010, *ApJ*, 714, L290
- Salpeter, E. E. 1955, *ApJ*, 121, 161
- Schlegel, D. J., Finkbeiner, D. P., & Davis, M. 1998, *ApJ*, 500, 525
- Seth, A. C., et al. 2010, *ApJ*, 714, 713
- Shen, J., & Sellwood, J. A. 2006, *MNRAS*, 370, 2
- Skrutskie, M. F., et al. 2006, *AJ*, 131, 1163
- Temi, P., Brighenti, F., & Mathews, W. G. 2009, *ApJ*, 695, 1
- Thilker, D. A., et al. 2010, *ApJ*, 714, L171
- Tikhonov, N. A., Galazutdinova, O. A., & Aparicio, A. 2003, *A&A*, 401, 863
- Tremonti, C. A., et al. 2004, *ApJ*, 613, 898
- van den Bergh, S. 2009, *ApJ*, 694, L120
- Verheijen, M. A. W. 2001, *ApJ*, 563, 694
- Wiklind, T., & Henkel, C. 1990, *A&A*, 227, 394
- Williams, B. F., et al. 2009a, *AJ*, 137, 419
- Williams, B. F., et al. 2009b, *ApJ*, 709, 135
- Wyder, T. K., et al. 2005, *ApJ*, 619, L15